Hindawi
International Journal of Photoenergy
Volume 2017, Article ID 5461030, 9 pages
https://doi.org/10.1155/2017/5461030

Research Article

Copper Sulfide Catalyzed Porous Fluorine-Doped Tin Oxide Counter Electrode for Quantum Dot-Sensitized Solar Cells with High Fill Factor

Satoshi Koyasu, Daiki Atarashi, Etsuo Sakai, and Masahiro Miyauchi

School of Materials and Chemical Technology, Tokyo Institute of Technology, 2-12-1 Ookayama, Meguro-ku, Tokyo 152-8552, Japan

Correspondence should be addressed to Masahiro Miyauchi; mmiyauchi@ceram.titech.ac.jp

Received 3 October 2016; Revised 7 January 2017; Accepted 10 January 2017; Published 26 January 2017

Academic Editor: Nini R. Mathews

The performance of quantum dot-sensitized solar cell (QDSSC) is mainly limited by chemical reactions at the interface of the counter electrode. Generally, the fill factor (FF) of QDSSCs is very low because of large charge transfer resistance at the interface between the counter electrode and electrolyte solution containing redox couples. In the present research, we demonstrate the improvement of the resistance by optimization of surface area and amount of catalyst of the counter electrode. A facile chemical synthesis was used to fabricate a composite counter electrode consisting of fluorine-doped tin oxide (FTO) powder and CuS nanoparticles. The introduction of a sputtered gold layer at the interface of the porous-FTO layer and underlying glass substrate also markedly reduced the resistance of the counter electrode. As a result, we could reduce the charge transfer resistance and the series resistance, which were 2.5 [Ω] and 6.0 [Ω], respectively. This solar cell device, which was fabricated with the presently designed porous-FTO counter electrode as the cathode and a PbS-modified electrode as the photoanode, exhibited a FF of 58%, which is the highest among PbS-based QDSSCs reported to date.

1. Introduction

The first quantum dot-sensitized solar cell (QDSSC) was reported over two decades ago [1]. Although QDSSCs have a similar structure and working principle to those of dye-sensitized solar cells (DSSCs), they have attracted considerable attention because of several advantageous characteristics, particularly a tunable bandgap in response to particle size, high visible-light absorbance, and possibility of multiple exciton generation [1, 2]. Recently, the high energy conversion efficiencies of QDSSC have been reported for PbS [3, 4] quantum dots (QD) and $CdSe_xTe_{1-x}$ QD [5] with ZnS shell. These QDSSCs exhibited higher short circuit current (J_{sc}) than a DSSC due to their absorption of a wider range of visible light and higher quantum yield. In contrast, the open circuit voltage (V_{oc}) of QDSSCs is only approximately 0.5 V. Therefore, the QDSSCs generally have high J_{sc} but have low V_{oc}. Under the condition with high J_{sc} and low V_{oc} properties, the fill factor (FF) of QDSSCs is highly sensitive to series resistance, as compared to solar cells with low J_{sc} and high V_{oc}. The FF of QDSSCs is reportedly limited by series resistance at the interface of the counter electrode [6, 7]. Consequently, the low V_{oc} and insufficient FF of QDSSCs limit their energy conversion efficiency of solar cells [8].

QDSSCs mainly consist of three components: a quantum dot-modified mesoporous TiO_2 electrode, which functions as a photoanode; a counter electrode, which functions as a cathode; and electrolyte, which is composed of sulfur redox couples and fills the gap between the photoanode and cathode. QDSSC involves several types of resistance, those in bulk or at interfaces. In particular, high resistance at the counter electrode limits the FF and efficiency of QDSSCs [9–11].

Two types of series resistance occur at counter electrodes: normal series resistance (R_s) and charge transfer resistance (R_{ct}). R_{ct} values are strongly dependent on the reduction reaction of the redox couple. Iodine redox couple is usually used in DSSCs system, while $S^{2-}/S_x{}^{2-}$ redox couple is used

in QDSSCs system. R_{ct} of $S^{2-}/S_x{}^{2-}$ redox couple in QDSSCs is markedly higher than that of the iodine redox couple in DSSCs because of lower reactivity of $S^{2-}/S_x{}^{2-}$ redox couple. Many researchers have attempted to develop efficient counter electrodes with low resistance for the construction of high FF solar cells. For example, Hodes et al. reported a low-resistance Cu_2S counter electrode, which was prepared by the sulfurization of a metallic copper sheet in polysulfide solution [12]. Also, some recent studies reported the counter electrodes with high surface area and low R_{ct} [13–23]. The origin of R_{ct} is the limitation of the chemical reaction for redox couple on the surface of electrode. Chemical reaction rate strongly depends on catalytic activity and surface area of a counter electrode. Therefore, porous structure with large surface area would have advantage to reduce R_{ct}. In particular, we have focused on the catalyst deposited porous oxide conductor as a counter electrode, which possesses high chemical stability, mechanical strength, catalytic activity, and conductivity. Although recent previous work reported the CuS deposited porous tin-doped indium oxide (ITO) counter electrode [24], optimizations of materials and structural parameters on theses electrodes, such as materials of porous layer, thickness of porous layer, loading amount of CuS catalyst, and the reduction of sheet resistance in a conductive substrate, are still challenging issues for the development of efficient QDSSCs.

In the present study, we aimed to develop the efficient counter electrode of QDSSCs with low R_{ct} as well as low R_s. To achieve low R_{ct}, we designed CuS deposited porous fluorine-doped tin oxide (FTO) electrodes by optimizing the thickness of porous-FTO layer and amount of CuS catalyst. We choose FTO but not ITO as porous layer because conductivity of ITO is extremely reduced by heating. To reduce R_s of electrodes, on the other hand, the reduction of sheet resistance in conductive substrate is very effective, since that of commercial FTO glass is relatively high (about 10 Ω/□). Generally, the sheet resistance of metal is lower than that of a commercial FTO glass, but only noble metals like gold (Au) or platinum (Pt) are available as a counter electrode of QDSSCs to avoid their corrosion in polysulfide electrolyte solution. However, use of these noble metals as a bulk form is not economical; thus, we introduced a thin Au layer between a commercial FTO glass and porous-FTO layer by sputtering to reduce R_s value. We developed CuS deposited porous-FTO film with underlying thin Au layer as an efficient counter electrode of QDSSC, which yielded quite high fill factor (FF = 58%).

2. Materials and Methods

2.1. Materials. Commercial FTO-coated glass substrates (AGC, sheet resistance: 10.2 Ω/□) were used for the fabrication of counter and working electrodes. Pt and Au discs were used as sputtering target materials and were purchased from Kojundo Chemical Laboratory. TiO_2 particles (P25, Degussa) were used for screen printing in the preparation of photoanodes. $Pb(CH_3COO)_2{\cdot}3H_2O$, $Zn(CH_3COO)_2{\cdot}2H_2O$, $Cu(CH_3COO)_2{\cdot}H_2O$, and $Na_2S{\cdot}9H_2O$ were purchased from Kanto Chemical. Tin chloride ($SnCl_4{\cdot}5H_2O$) and ammonia aqueous solution (NH_3 aq (25%)) were also purchased from Kanto Chemical, and acetylene carbon black was obtained from Sigma-Aldrich.

2.2. Fabrication of Counter Electrode. FTO nanopowder was synthesized according to a previously described procedure [25]. Briefly, 14.02 g $SnCl_4{\cdot}5H_2O$, 0.704 g NH_4F, and 0.8 g acetylene carbon black were mixed with 40 mL distilled water in a beaker. Ammonia aqueous solution (25%) was then added until the pH of the solution reached 7. The resulting gel was dried at 100°C for 1 day and was then heated at 650°C for 30 min. After the heating treatment, the obtained powder was further annealed at 750°C for 30 min and was then immersed in pure water. The dispersed FTO particles were collected by centrifugation (6000 rpm for 5 min) and were mixed with ethyl cellulose and α-terpineol to prepare a paste for screen printing. For preparation of the FTO paste, 2 g FTO powder was dispersed in 200 mL ethanol, to which 6 mL ethyl cellulose solution was added. The ethyl cellulose solution was prepared by mixing two different molecular weights of ethyl cellulose (30–60 mPa s: 0.333 g + 5–15 mPa s: 0.666 g) in 10 mL ethanol. Following the addition of ethyl cellulose, 4 mL α-terpineol was added to FTO dispersed solution. After stirring for 10 min, ethanol was evacuated using an evaporator at 50°C to obtain FTO paste. Porous-FTO electrodes were constructed by screen-printing the FTO paste on a commercial dense FTO-coated glass, which was subsequently sintered at 450°C for 30 min. The thickness of the porous-FTO layers was controlled by the mesh size of the screen mask and the number of screen coating times. Using this method, porous-FTO electrodes with thicknesses of 5, 10, 15, and 20 μm were fabricated. We have optimized the thickness to obtain the low resistance as mentioned later. Subsequently, CuS catalyst nanoparticles were loaded onto the constructed porous-FTO electrodes by a successive ionic layer adsorption and reaction (SILAR) method [26, 27]. Two types of aqueous solutions, 0.1 M copper acetate ($Cu(CH_3COO)_2$) and 0.1 M sodium sulfide (Na_2S), were prepared for the SILAR method. Porous-FTO electrodes were immersed in $Cu(CH_3COO)_2$ solution for 30 sec and were then washed with distilled water. The washed substrates were immersed in Na_2S solution for 30 sec, followed by washing with distilled water. The dipping cycles in the two solutions were repeated 5 to 40 times, and the substrates were then dried at room temperature for 1 h. According to the SILAR cycles, we could optimize the loading amount of CuS. In addition to the fabrication of CuS-modified counter electrodes, a powder form of CuS was prepared using the same solutions with the SILAR method for XRD analysis, as the amount and crystallite size of CuS on porous-FTO were too small to determine the crystal phase of CuS.

To investigate the effect of a metal-conducting layer between the dense FTO film and porous-FTO layer, Au thin film was coated on the surface of a commercial FTO glass substrate by DC magnetron sputtering (MSP-30T; Vacuum Device) before the screen printing of the porous-FTO layer. Au was deposited for 3 min at a current of 200 mA under an argon atmosphere pressure of 8.1×10^{-4} Pa. Under these conditions, the thickness of the resulting Au layer was

350 nm, as estimated by the deposition rate and sputtering time. The expected resistance of our Au layer was calculated by considering the electrode structure. The distance from porous-FTO to the position for bonding attaching clip was 15 mm. The width of porous-FTO was 5 mm, and resistivity of gold was about 2×10^{-8} [Ωm]. If we use gold thin film of 350 nm, calculated expected resistance of gold layer by using these values is calculated as 2×10^{-8} [Ωm] $\times 15 \times 10^{-3}$ [m]/(5×10^{-3} [m] $\times$ 350 $\times 10^{-9}$ [m]) = 0.17 [Ω]. For comparison with a conventional counter electrode that is typically used in QDSSCs and DSSC, platinum (Pt) counter electrodes were prepared by sputtering of Pt (MSP-30T; Vacuum Device) onto a commercial FTO-coated glass substrate at 200 mA for 45 sec at a pressure of 8.1×10^{-4} Pa.

2.3. Fabrication of PbS Photoanode. A photoanode was fabricated using a previously reported method [4]. Briefly, TiO_2 paste was prepared from commercial TiO_2 powder (P-25, Degussa) by mixing with ethyl cellulose and α-terpineol. Typically, 1 g TiO_2 powder was dispersed in 200 mL ethanol containing two types of ethyl cellulose with different viscosities, as was described for the FTO paste fabrication. After stirring the solution for 10 min, ethanol was evacuated using an evaporator at 50°C. Porous TiO_2 electrodes were then constructed on commercial dense FTO-coated glass by the screen printing of the TiO_2 paste and subsequent sintering at 450°C for 30 min.

Core-shell-type PbS/ZnS QDs were deposited on the porous TiO_2 electrode using the SILAR method. Previous studies have reported that the ZnS shell prevents the back electron transfer and recombination of electron on the surface of PbS light absorber [4, 28]. QD-modified photoanodes were also prepared by the SILAR method. Two types of solutions, 0.02 M of lead acetate ($Pb(CH_3COO)_2$) dissolved in methanol and 0.02 M of sodium sulfide (Na_2S) in methanol, were used for PbS QD deposition onto porous TiO_2 electrodes. First, porous TiO_2 electrodes were immersed in $Pb(CH_3COO)_2$ solution for 30 sec and washed once with methanol, and the electrodes were then immersed in Na_2S solution for 30 sec, followed by a further wash with methanol. The dipping cycles in the two solutions were repeated twice. In addition to PbS QD deposition, a ZnS thin layer was formed on the surface of the PbS QDs to form a core-shell structure. To form the ZnS thin layer, the PbS-modified TiO_2 electrodes were immersed in 0.02 M of zinc acetate ($Zn(CH_3COO)_2$) in methanol solution for 30 sec, washed once with methanol, and then dipped in 0.02 M of Na_2S methanol solution for 30 sec, followed by a further wash with methanol. The dipping cycles were repeated for 10 times, resulting in the formation of ZnS shells on the PbS QDs. After completion of the SILAR cycles, the substrates were dried at room temperature for 1 h.

2.4. Characterization and Electrochemical Properties of Counter Electrode. The crystal phase of synthesized FTO powder was determined using a X-ray diffraction meter (XRD; Rigaku SmartLab SPI/TISM). Morphologies of the surface and cross section of the porous-FTO electrodes were recorded using a field emission scanning electron microscope (FE-SEM; Hitachi S4500). Microstructures of CuS/FTO composites removed from the electrodes by scraping were observed using a JEM-2010F transmission electron microscope (TEM; JEOL, Ltd.). The specific surface area (BET) of the porous-FTO electrode was also measured by determination of the nitrogen adsorption-desorption isotherm using a surface area analyzer (Gemini V 2380; Shimadzu Corp.).

Catalytic performance of counter electrodes was studied by conducting electrochemical impedance analysis. Impedance analysis is one of the most useful methods to separately discuss the charge transfer resistance and normal series resistance. For the analysis, the CuS-modified FTO electrode was connected as a working electrode, and the Pt and Ag/AgCl electrodes were used as counter and reference electrodes, respectively. Catalytic activities of CuS-modified FTO electrodes were investigated by measuring series resistance (R_s) and charge transfer resistance (R_{ct}), which were determined from fitting results of Nyquist plots. A potentiostat equipped with a frequency response analyzer (FRA) was used for impedance measurements (HZ-5000; Hokuto Denko). In the electrochemical measurements, the area of the electrode exposed to the electrolyte solution was 0.25 cm^2, and the bias was set at the rest potential condition (0.67 V versus Ag/AgCl), amplitude voltage was 10 mV, and the AC frequency ranged from 20 kHz to 0.01 Hz. The electrolyte was composed of 1.0 M Na_2S and 1.0 M sulfur aqueous solution.

2.5. Fabrication and Performance Evaluation of Solar Cell Device. An aqueous solution composed of 1.0 M sodium sulfide and 1.0 M sulfur was used as an electrolyte in the QDSSC device, which contained a 50 μm gap between the CuS counter electrode and PbS photoanode due to the insertion of an ethylene polymer film spacer (Surlyn; Du Pont, Ltd.).

The electrolyte solution was introduced into the gap between the counter electrode and photoanode through two pinholes that were made in the FTO glass counter electrode using an ultrasonic pinhole maker. After introducing the electrolyte solution into the gap, the pinholes in the counter electrode were covered with masking tape. A solar simulator (Peccell Ltd.) was used to measure the efficiency and FF of the solar cell. Incident photon to current conversion efficiency (IPCE) was measured using a SM-250 DAM (Bunko Keiki Ltd.). A schematic illustration of the solar cell configuration is shown in Figure 1.

3. Results and Discussion

The crystal phase of the synthesized FTO powder was investigated by XRD (Figure 2). All XRD diffraction peaks of the FTO powder were assigned to rutile SnO_2 (ICDD number 01-076-7837, space group: P42/mnm).

UV-Vis diffuse reflectance spectra of the FTO powder revealed that fluorine doping resulted in broad visible-light absorption, indicating that free electrons were formed

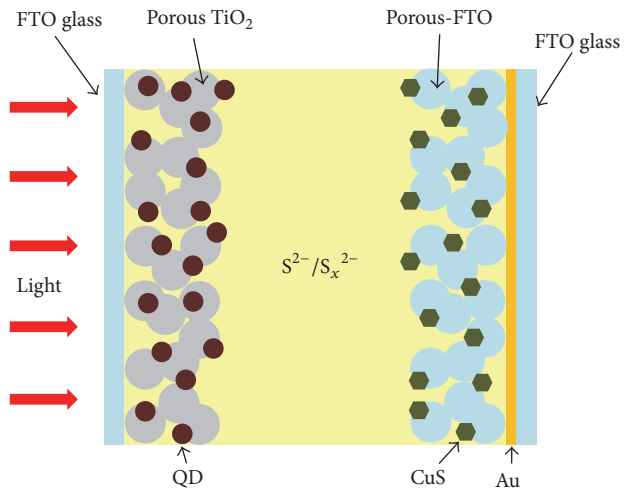

FIGURE 1: Schematic illustration of a QDSSC equipped with a porous-FTO/CuS counter electrode.

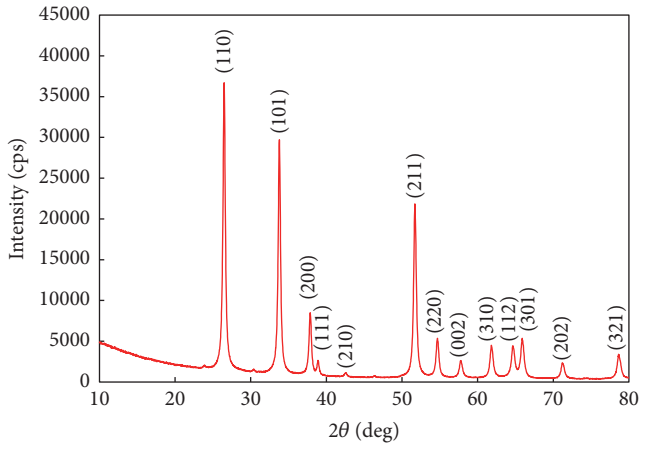

FIGURE 2: XRD pattern of FTO powder.

in the SnO_2 crystal (see the supporting information, Figure S1, in Supplementary Material available online at https://doi.org/10.1155/2017/5461030). Surface area of porous-FTO (thickness 5 μm) was determined by nitrogen adsorption-desorption isotherm. This value was 286 cm^2/cm^2 (real surface area/apparent surface area).

Photographs of the fabricated porous-FTO/CuS counter electrodes were shown in our supporting information (Figure S3), in which one electrode was constructed with an Au film between the porous-FTO and commercial FTO glass substrate, and another was constructed without an Au layer. A cross-sectional SEM image of the counter electrode is shown in Figure 3(a). From the image, it was determined that the thickness of the porous-FTO layer loaded with CuS catalyst was 5 μm, and this layer was uniformly coated on the commercial FTO glass substrate. CuS was deposited on the substrate using 20 SILAR cycles, which was determined to be optimum for this solar cell device, as described in detail below. As the CuS nanoparticles could not be clearly observed by SEM, the CuS/FTO composite was analyzed by TEM after being scraped from the surface of the counter electrode. Two sizes of particles were observed in the composite: 10 to 20 nm particles (i) with anisotropic shape and 50 nm particles (ii) with spherical shape (Figure 3(b)). To determine the microstructure of the CuS/FTO composite, EDX point analysis was performed (Figure 3(c)). The analysis indicated that the 10 to 20 nm particles (i) were CuS catalyst, whereas the 50 nm spherical particles (ii) were FTO. The CuS particles were highly dispersed and attached onto the FTO surface of the electrode. We also investigated the XRD pattern for CuS powder synthesized by the same starting solution of the SILAR method, and all diffraction peaks were assigned to covellite CuS crystal phase (see our supporting information, Figure S4).

We optimized various parameters, including loading amount of CuS, porous-FTO thickness, and Au layer insertion on the substrate. R_s, R_{ct}, and internal resistance (R_{in}) values were determined from fitting results using the equivalent circuit (Figure S5 in supporting information). We used an inductance in the equivalent circuit, because we used thin conducting wire which have small inductance for impedance measurement. Constant phase element (CPE) contains two parameters T and P. Impedance (Z) of CPE was defined by the equation $Z = 1/(T \times (i\omega)^P)$. In our electrode, CPE1-T value (like a capacitance) was smaller than CPE2-T value. Therefore, R_{in} was attributed to the high-frequency semicircle, and R_{ct} was attributed to the low-frequency semicircle. Figures 4(a)(1), 4(a)(2), 4(a)(3), and 4(a)(4) are Nyquist plots of the samples fabricated by SILAR cycle 5, 10, 20, and 40 times with a thickness of 5 μm for porous-FTO. Two semicircles were observed in the plots of all samples. Figure 4(b) shows the influence of the number of SILAR cycles used for CuS deposition on the resistance derived from the semicircles in Figure 4(a). Although the internal resistance (R_{in}) and R_s values were not markedly affected by the number of SILAR cycles, R_{ct} was decreased with increasing number of SILAR cycles. The reduction of R_{ct} was saturated at approximately 15 Ω when 20 SILAR cycles were used for CuS deposition. Warburg Impedance (W_o) was decreased with increasing number of SILAR cycles. The origin of W_o is attributed to diffusion of S_x^{2-} redox, and the decrease of W_o would be owing to the efficient reduction reaction of S_x^{2-} at CuS sites. The electrode of 40 SILAR cycles exhibited the lowest W_o resistance, but the electrode of 20 SILAR cycles also exhibited sufficiently low resistance. Additionally, the film of 40 SILAR cycles was unstable and easily peeled off, since inner pressure was increased by excessive crystal growth of CuS by SILAR (Figure S2).

Based on the optimization of loading amount of CuS, we used the electrode with 20 SILAR cycles for achieving the low resistance of the porous-FTO/CuS electrodes. The origin of R_{ct} was attributed to the resistance of charge transfer between CuS and electrolyte, because R_{ct} was decreased with increasing number of SILAR cycles. In contrast, R_{in} was not so affected by SILAR cycle, since R_{in} was attributed to resistance of CuS/FTO interface or grain boundary of FTO particles.

The influence of the porous-FTO film thickness on resistance was next examined using porous-FTO/CuS electrodes

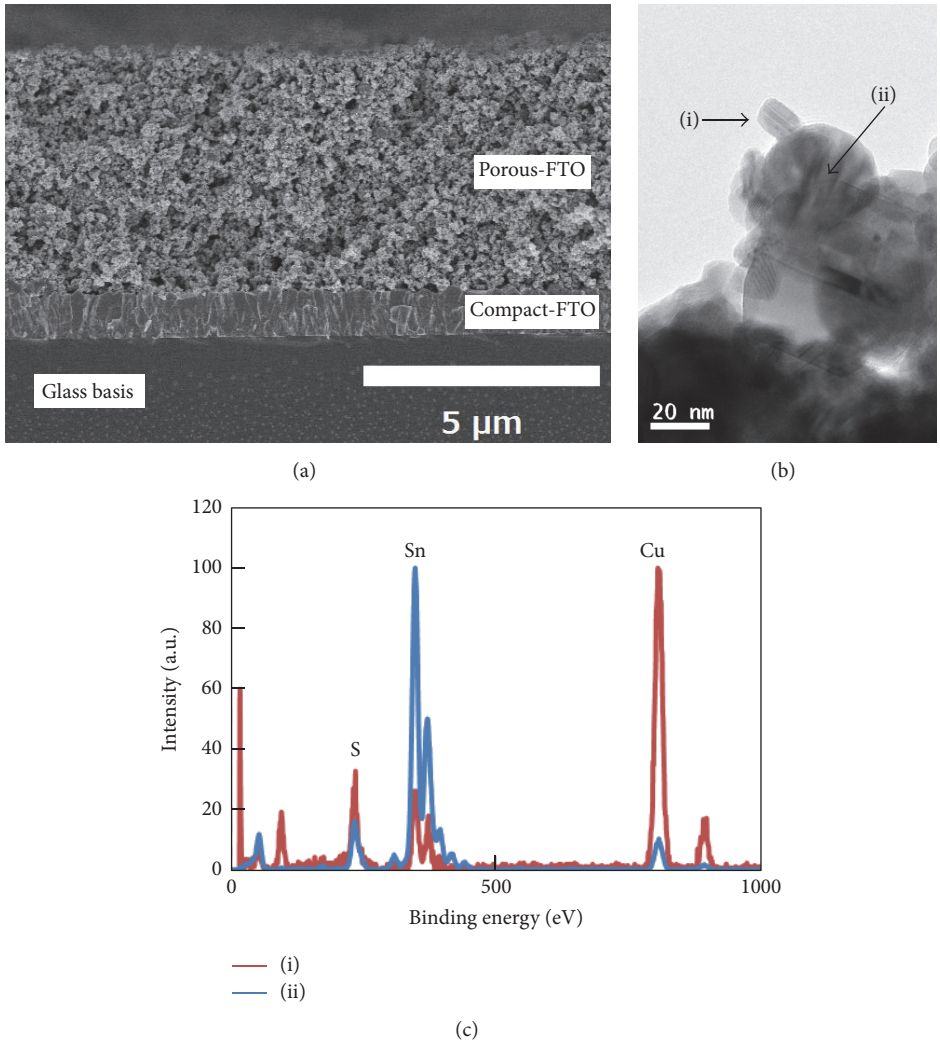

Figure 3: Cross-sectional SEM image of a porous-FTO electrode (a), TEM image of the porous-FTO (ii)/CuS (i) composite removed from the counter electrode surface (b), and EDX point analysis at points (i) and (ii) in the TEM image (c).

constructed using 20 CuS SILAR cycles. Nyquist plots of electrodes with porous-FTO films ranging from 5, 10, 15, and 20 μm are shown in Figures 5(a)(1), 5(a)(2), 5(a)(3), and 5(a)(4) and the thickness dependence on the resistance is shown in Figure 5(b). In contrast to R_{in} and W_o, R_{ct} was significantly decreased when the thickness of porous-FTO layer was increased. The decrease of R_{ct} is attributable to the increase of the electrode surface area that is available to drive catalytic reactions. R_{in} and W_o were slightly increased with increasing thickness of porous-FTO. We speculate that the increase of R_{in} was caused by grain boundaries in porous-FTO as increase of FTO thickness, and W_o was also increased by blocking effect of S_x^{2-} ion diffusion in thick porous structure. As the reduction of resistance was saturated around 20 μm, we concluded that the optimum structural condition for the QDSSC counter electrode is a porous-FTO layer of 20 μm thickness and 20 SILAR cycles for CuS deposition.

We speculate that the CuS exhibited high catalytic activity for the reduction of S^{2-}/S_x^{2-} redox couples due to the efficient adsorption of S_2^{2-} ion onto CuS crystals. R_{ct} of the counter electrode is lower than that previously reported for counter electrodes containing CuS catalyst [13, 24], owing to our optimization of the CuS synthesis process. Specifically, we used copper acetate as a starting precursor for CuS synthesis, as the nucleation and crystal growth of metal sulfide particles are limited in strong acid conditions, such as nitrate and chloride salts. CuS has a unique crystal configuration, in which there are two types of sulfur sites, namely, S^{2-} and S_2^{2-} ions. Crystal structure of CuS (covellite) is shown in our supporting information (Figure S6). Notably, the solid-state S_2^{2-} site has structural similarity with the polysulfide ion in the electrolyte used in our system and plays an important role in the catalytic reactivity with sulfur redox couples in the electrolyte. We investigated the relationship between the crystal structures of various metal sulfide catalysts and their catalytic properties, and the data were shown in our supporting information (Figure S7). Among CuS, FeS_2, and PbS catalysts, CuS exhibited the highest redox efficiency.

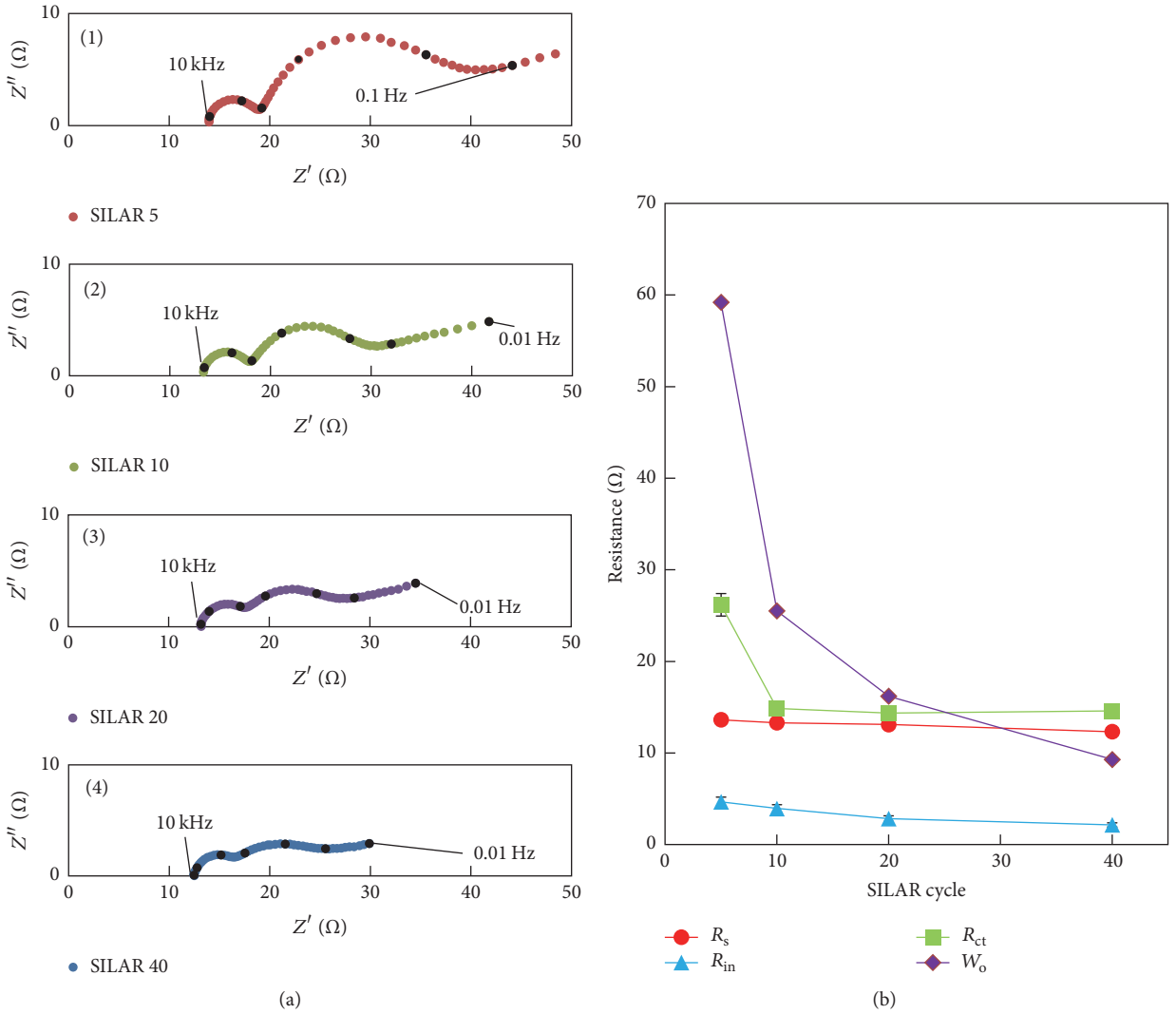

FIGURE 4: Nyquist plots of porous-FTO (5 μm)/CuS electrodes for various SILAR cycles. Panels (a)(1), (a)(2), (a)(3), and (a)(4) are the results for SILAR cycles with 5, 10, 20, and 40 times, respectively. SILAR cycles dependence on the resistance is shown in panel (b). Black dots in panels (a)(1) to (a)(4) indicate the data recorded under each decade of the frequency.

Notably, cathodic current densities of CuS and FeS_2 were higher than that of PbS. Both CuS and FeS_2 have S_2^{2-} sites in their crystal, while PbS does not. Further, we also compared our CuS loaded porous-FTO electrode with a conventional Pt counter electrode, and the conductivity of our electrode was much superior than that of a Pt electrode (see our supporting information, Figure S8). Electrodes' stability is very important for a practical application; thus, we studied the stability of the CuS-modified porous-FTO electrode under the repeated redox reaction for 20 cycles (supporting information, Figure S9). And, as a result, the performance of our electrode remained stable, suggesting its high stability under the repeated redox reactions.

We also investigated the effect of inserting a layer of Au between the dense FTO layer of commercial FTO-coated glass and the porous-FTO layer. Figures 6(a) and 6(b) show Nyquist plots for counter electrodes (20 SILAR cycles, 20 μm FTO layer) with and without an Au layer. The structural features of electrode, other than the Au layer, were fixed at using the optimal conditions described above. The introduction of the Au layer at the interface between the porous and dense FTO layers led to a drastic reduction in R_s. This result suggests that the sheet resistance of the dense FTO layer of commercial substrate is largely decreased by the sputtered Au layer. We have comprehensively designed and analyzed the nanostructure and interfaces of the counter electrode and concluded that a 20 μm porous-FTO layer, 20 SILAR cycles for CuS deposition, and the inclusion of an Au layer at the interface between the porous and dense FTO layers are optimal for decreasing the resistance of the counter electrode. Under these conditions, the lowest R_s, R_{in}, and R_{ct} values achieved were 2.52, 2.86, and 6.04 Ω, respectively.

We fabricated a sandwich-type solar cell device using the optimized counter electrode and PbS-modified photoanode. As a comparison, we also prepared a QDSSC with a Pt counter electrode. The *I-V* curves of the two QDSSCs under a 1.5

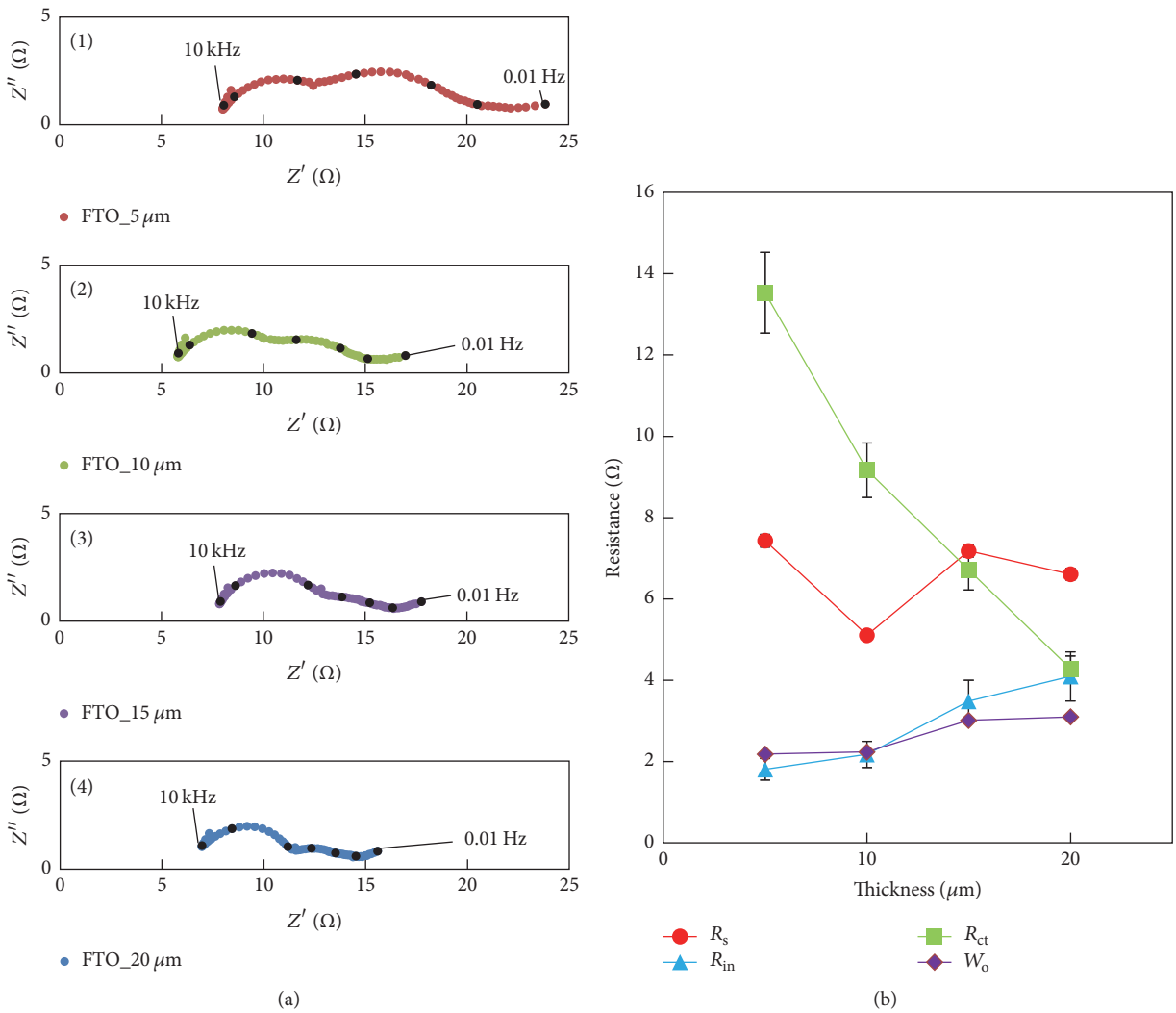

Figure 5: Nyquist plots for porous-FTO/CuS electrodes for various FTO thicknesses. Panels (a)(1), (a)(2), (a)(3), and (a)(4) are the results for FTO thicknesses of 5, 10, 15, and 20 μm, respectively. FTO thickness dependence on the resistance is shown in panel (b). CuS SILAR cycle for all samples was fixed at 20 times. Black dots in panels (a)(1) to (a)(4) indicate the data recorded under each decade of the frequency.

AM solar simulator are shown in Figure 7. The QDSSC with a Pt counter electrode exhibited very low FF (16%) and limited energy conversion efficiency (0.61%). In contrast, the QDSSC with the porous-FTO/CuS (thickness 5 μm, SILAR cycle 5) counter electrode exhibited relatively high FF (51.6%) and energy conversion efficiency (1.12%). The QDSSC with the optimized Au/porous-FTO/CuS (thickness 20 μm, SILAR cycle 20) counter electrode exhibited quite high FF (58%) and energy conversion efficiency (1.59%). Resistance values of counter electrodes and solar cells properties were summarized in Table 1. Notably, J_{sc} and V_{oc} were not influenced by the type of counter electrode but were affected by the photoanode, indicating that our optimized counter electrode could be used in devices constructed with other types of photoanodes, such as CdS/CdSe. J_{sc} and V_{oc} of the QDSSC with the Pt counter electrode were larger than those of the QDSSC constructed with the porous-FTO/CuS counter electrode. These results are due to differences in the reflectivity of the counter electrode, as the Pt electrode reflects more visible light back to the photoanode. However, if the amount of visible-light absorption by the photoanode is sufficient, the reflection from the counter electrode becomes negligible. Thus, the FF of QDSSC in the present study is the most efficient reported to date and is generally applicable for use with various types of photoanodes for the development of efficient QDSSCs with high FF.

Table 1: Resistance values and solar cell properties.

	R_s [Ω]	R_{in} [Ω]	R_{ct} [Ω]	J_{sc} [mA/cm^2]	V_{oc} [V]	FF [%]	η [%]
Pt	12.7		7519	8.80	0.43	16	0.61
CuS5/FTO5 μm	13.6	4.7	26.2	5.81	0.37	52	1.12
CuS20/FTO20 μm/Au	2.5	2.9	6.0	7.14	0.38	58	1.59

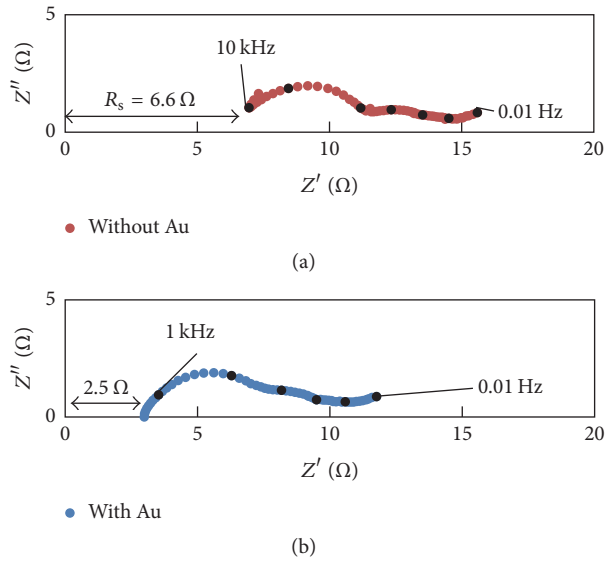

Figure 6: Nyquist plots of counter electrodes constructed without Au (a) and with Au layer (b). Black dots indicate the data recorded under each one decade of the frequency.

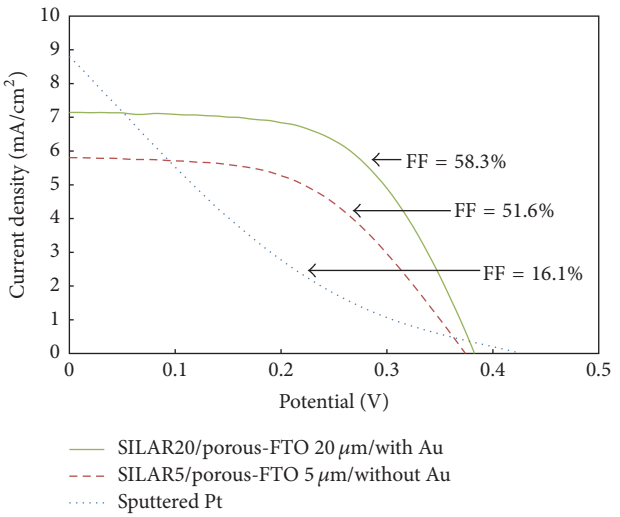

Figure 7: *I-V* curves of QDSSCs constructed with various counter electrodes under solar simulator. Blue dotted line: Pt counter electrode, red dashed line: porous-FTO/CuS (porous-FTO thickness: 5 μm, SILAR cycles: 5 times), and solid green line: Au/porous-FTO/CuS (porous-FTO thickness: 20 μm, SILAR cycles: 20 times), respectively.

4. Conclusions

We have fabricated the efficient counter electrode for constructing QDSSCs, on the basis of the CuS deposited porous-FTO electrode. According to the optimization on the thickness of porous-FTO layer and loading amount of CuS nanoparticles, R_{ct} value was drastically decreased. We also found that introduction of an Au layer between the porous-FTO layer and dense FTO led to a marked reduction in R_s. Finally, very low R_s (2.5 Ω) and R_{ct} (6.0 Ω) were achieved. When we combined the optimized counter electrode with a PbS-based photoanode, the highest FF (58%) was achieved among previously reported PbS and polysulfide electrolyte based QDSSCs. Our CuS-modified porous-FTO counter electrode can be combined with various types of photoanodes, in addition to PbS-based photoanodes. The strategy to design the counter electrode is expected to be applicable for other types of QDs for the development of QDSSCs with even higher efficiency.

Competing Interests

The authors declare that they have no competing interests.

Acknowledgments

This work is financially supported by JST PRESTO, JST ACT-C programs, and JSPS KAKENHI Grant no. 26410234. The authors also thank Mr. J. Koki and Mr. A. Genseki for electron microscope observation. The manuscript was carefully read by Mr. G. Newton.

References

[1] R. Vogel, K. Pohl, and H. Weller, "Sensitization of highly porous, polycrystalline TiO_2 electrodes by quantum sized CdS," *Chemical Physics Letters*, vol. 174, no. 3-4, pp. 241–246, 1990.

[2] Y. Wang, A. Suna, W. Mahler, and R. Kasowski, "PbS in polymers. From molecules to bulk solids," *The Journal of Chemical Physics*, vol. 87, no. 12, pp. 7315–7322, 1987.

[3] S. D. Sung, I. Lim, P. Kang, C. Lee, and W. I. Lee, "Design and development of highly efficient PbS quantum dot-sensitized solar cells working in an aqueous polysulfide electrolyte," *Chemical Communications*, vol. 49, no. 54, pp. 6054–6056, 2013.

[4] S. Hachiya, Q. Shen, and T. Toyoda, "Effect of ZnS coatings on the enhancement of the photovoltaic properties of PbS quantum dot-sensitized solar cells," *Journal of Applied Physics*, vol. 111, no. 10, Article ID 104315, 2012.

[5] Z. Pan, K. Zhao, J. Wang, H. Zhang, Y. Feng, and X. Zhong, "Near infrared absorption of CdSexTe1-x alloyed quantum dot sensitized solar cells with more than 6% efficiency and high stability," *ACS Nano*, vol. 7, no. 6, pp. 5215–5222, 2013.

[6] J. G. Radich, R. Dwyer, and P. V. Kamat, "Cu_2S reduced graphene oxide composite for high-efficiency quantum dot solar cells. Overcoming the redox limitations of S_2^-/S_n^{2-} at the counter electrode," *The Journal of Physical Chemistry Letters*, vol. 2, no. 19, pp. 2453–2460, 2011.

[7] Y. Jiang, X. Zhang, Q. Q. Ge et al., "ITO@Cu2S tunnel junction nanowire arrays as efficient counter electrode for quantum-dot-sensitized solar cells," *Nano Letters*, vol. 14, no. 1, pp. 365–372, 2014.

[8] M. Wolf and H. Rauschenbach, "Series resistance effects on solar cell measurements," *Advanced Energy Conversion*, vol. 3, no. 2, pp. 455–479, 1963.

[9] J. Jiao, Z.-J. Zhou, W.-H. Zhou, and S.-X. Wu, "CdS and PbS quantum dots co-sensitized TiO2 nanorod arrays with improved performance for solar cells application," *Materials Science in Semiconductor Processing*, vol. 16, no. 2, pp. 435–440, 2013.

[10] L. Meng, F. Zhao, J. Zhang et al., "Preparation of monodispersed PbS quantum dots on nanoporous semiconductor thin film by

two-phase method," *Journal of Alloys and Compounds*, vol. 595, pp. 51–54, 2014.

[11] A. N. Jumabekov, F. Deschler, D. Böhm, L. M. Peter, J. Feldmann, and T. Bein, "Quantum-dot-sensitized solar cells with water-soluble and air-stable PbS quantum dots," *The Journal of Physical Chemistry C*, vol. 118, no. 10, pp. 5142–5149, 2014.

[12] G. Hodes, J. Manassen, and D. Cahen, "Electrocatalytic electrodes for the polysulfide redox system," *Journal of the Electrochemical Society*, vol. 127, no. 3, pp. 544–549, 1980.

[13] W. Ke, G. Fang, H. Lei et al., "An efficient and transparent copper sulfide nanosheet film counter electrode for bifacial quantum dot-sensitized solar cells," *Journal of Power Sources*, vol. 248, pp. 809–815, 2014.

[14] K. Zhao, H. Yu, H. Zhang, and X. Zhong, "Electroplating cuprous sulfide counter electrode for high-efficiency long-term stability quantum dot sensitized solar cells," *The Journal of Physical Chemistry C*, vol. 118, no. 11, pp. 5683–5690, 2014.

[15] S.-Q. Fan, B. Fang, J. H. Kim, J.-J. Kim, J.-S. Yu, and J. Ko, "Hierarchical nanostructured spherical carbon with hollow core/mesoporous shell as a highly efficient counter electrode in CdSe quantum-dot-sensitized solar cells," *Applied Physics Letters*, vol. 96, no. 6, Article ID 063501, 2010.

[16] M. Seol, D. H. Youn, J. Y. Kim et al., "Mo-compound/CNT-graphene composites as efficient catalytic electrodes for quantum-dot-sensitized solar cells," *Advanced Energy Materials*, vol. 4, no. 4, Article ID 1300775, 2014.

[17] S.-Q. Fan, B. Fang, J. H. Kim et al., "Ordered multimodal porous carbon as highly efficient counter electrodes in dye-sensitized and quantum-dot solar cells," *Langmuir*, vol. 26, no. 16, pp. 13644–13649, 2010.

[18] Z. Tachan, M. Shalom, I. Hod, S. Rühle, S. Tirosh, and A. Zaban, "PbS as a highly catalytic counter electrode for polysulfide-based quantum dot solar cells," *Journal of Physical Chemistry C*, vol. 115, no. 13, pp. 6162–6166, 2011.

[19] E. Ramasamy, W. J. Lee, D. Y. Lee, and J. S. Song, "Spray coated multi-wall carbon nanotube counter electrode for tri-iodide (I3-) reduction in dye-sensitized solar cells," *Electrochemistry Communications*, vol. 10, no. 7, pp. 1087–1089, 2008.

[20] H. Yu, H. Bao, K. Zhao, Z. Du, H. Zhang, and X. Zhong, "Topotactically grown bismuth sulfide network film on substrate as low-cost counter electrodes for quantum dot-sensitized solar cells," *The Journal of Physical Chemistry C*, vol. 118, no. 30, pp. 16602–16610, 2014.

[21] M.-H. Yeh, C.-P. Lee, C.-Y. Chou et al., "Conducting polymer-based counter electrode for a quantum-dot-sensitized solar cell (QDSSC) with a polysulfide electrolyte," *Electrochimica Acta*, vol. 57, no. 1, pp. 277–284, 2011.

[22] Q. Zhang, Y. Zhang, S. Huang et al., "Application of carbon counterelectrode on CdS quantum dot-sensitized solar cells (QDSSCs)," *Electrochemistry Communications*, vol. 12, no. 2, pp. 327–330, 2010.

[23] Y. Jiang, X. Zhang, Q.-Q. Ge et al., "Engineering the interfaces of ITO@Cu2S nanowire arrays toward efficient and stable counter electrodes for quantum-dot-sensitized solar cells," *ACS Applied Materials & Interfaces*, vol. 6, no. 17, pp. 15448–15455, 2014.

[24] H. Chen, L. Zhu, H. Liu, and W. Li, "ITO porous film-supported metal sulfide counter electrodes for high-performance quantum-dot-sensitized solar cells," *The Journal of Physical Chemistry C*, vol. 117, no. 8, pp. 3739–3746, 2013.

[25] C.-H. Han, S.-D. Han, J. Gwak, and S. P. Khatkar, "Synthesis of indium tin oxide (ITO) and fluorine-doped tin oxide (FTO) nano-powder by sol–gel combustion hybrid method," *Materials Letters*, vol. 61, no. 8-9, pp. 1701–1703, 2007.

[26] Y. F. Nicolau, "Solution deposition of thin solid compound films by a successive ionic-layer adsorption and reaction process," *Applications of Surface Science*, vol. 22-23, no. 2, pp. 1061–1074, 1985.

[27] Y. F. Nicolau, M. Dupuy, and M. Brunel, "ZnS, CdS, and $Zn_{1-x}Cd_xS$ thin films deposited by the successive ionic layer adsorption and reaction process," *Journal of the Electrochemical Society*, vol. 137, no. 9, pp. 2915–2924, 1990.

[28] B. O. Dabbousi, J. Rodriguez-Viejo, F. V. Mikulec et al., "(CdSe)ZnS core-shell quantum dots: synthesis and characterization of a size series of highly luminescent nanocrystallites," *Journal of Physical Chemistry B*, vol. 101, no. 46, pp. 9463–9475, 1997.